Adaptive Two-Step Peer Methods for Thermally Coupled Incompressible Flow

Bettina Gottermeier*, Jens Lang
*gottermeier@mathematik.tu-darmstadt.de

TECHNISCHE
UNIVERSITÄT
DARMSTADT

Research Group
Numerical Analysis and
Scientific Computing

Abstract

In the present paper, we apply two-step peer methods up to order five to thermally coupled incompressible flow. These methods were first developed for ODEs and subsequently applied to parabolic PDEs. Because of their linearly implicit character only linear systems have to be solved in each time step. Additionally, good stability properties are given by optimal zero-stability and $L(\alpha)$-stability with an angle of at least $\alpha = 85°$. The main advantage over one-step methods lies in the fact that even in the application to PDEs no order reduction is observed. To investigate whether the higher order of convergence of the two-step peer methods equipped with variable time steps pays off in practically relevant CFD computations, we apply the peer methods to a typical benchmark problem, the thermo-convective instability of plane Poiseuille flow, and study the accuracy and efficiency of these methods. Comparisons are made with linearly implicit one-step methods of Rosenbrock-type with classical order two and three. The two-step methods are highly accurate and more efficient than one-step Rosenbrock methods, in particular than Ros2, which is similar to the well-known Crank-Nicolson method.

1 INTRODUCTION

A numerical study of a benchmark problem for thermally coupled incompressible flows [1, 4] is presented in this paper. The problem consists of a two-dimensional laminar flow in a rectangular domain, which is suddenly heated from below and results in a thermo-convective instability. Besides the practical interest in this benchmark problem, the system of nonlinear equations forms a very good test case for numerical methods as instabilities and even transition to turbulence can occur in these flows [1].

Following the Rothe method, the system of nonlinear equations is first discretized in time. Explicit or simple implicit numerical methods as the backward Euler method, the Crank-Nicolson method or the fractional-step θ-method are widely-used to approximate the temporal evolution of incompressible flows. Besides their low order of convergence, it is difficult to realize an adaptive time step control which increases the efficiency of these methods [7]. In this paper, linearly implicit two-step peer methods [5] of higher order equipped with variable time steps are used to discretize the nonlinear equations in time. Such methods take a linear combination of stage values to approximate the exact solution at intermediate points. All of these stage values have the same order of accuracy and the same stability properties, which is the reason for calling the methods 'peer'. The methods considered here are up to fifth order accurate and exhibit good stability properties with optimal zero-stability and $L(\alpha)$-stability with a large angle α. They are robust with respect to step size changes due to the strong damping property at infinity. Because of their linearly implicit structure, only linear systems have to be solved in each time step. Even in the application to PDEs, the peer methods do not suffer from order reduction, which is the main advantage over one-step methods. Additionally, they have shown a superior performance with respect to accuracy and efficiency compared to one-step methods [5, 6].

The outline of the present paper reads as follows: We introduce the benchmark problem of the thermo-convective instability of plane Poiseuille flow in Sect. 2. Then, in Sect. 3, the resulting system of nonlinear equations is discretized in time with linearly implicit two-step peer methods. For the space discretization, a stabilized finite element method based on piecewise linear elements for the velocity, pressure, and temperature is used. The time-adaptive simulations are performed with the software package KARDOS [3], whose results are presented in Sect. 4. Finally, a summary of our results and conclusion can be found in Sect. 5.

2 PROBLEM DESCRIPTION

We consider a two-dimensional thermally coupled incompressible flow in a horizontal channel $\Omega = [0, 10] \times [0, 1]$, which has been proposed as a benchmark problem for open boundary flows by Evans and

Paolucci [4]. These flows are modelled by the well-known Navier-Stokes equations with the Boussinesq approximation for the thermal coupling given in dimensionless form by

$$\partial_t u + (u \cdot \nabla)u - Re^{-1}\Delta u + \nabla p = -Fr^{-1}T\hat{g}\,, \tag{2.1a}$$

$$\nabla \cdot u = 0\,, \tag{2.1b}$$

$$\partial_t T + (u \cdot \nabla)T - Pe^{-1}\Delta T = 0\,, \qquad x \in \Omega\,, \quad t \in (0, t_e]\,. \tag{2.1c}$$

The vector $u = (u_1, u_2)^T \in \mathbb{R}^2$ is the velocity field, the scalar p and T are the pressure and temperature. The system of equations has to be equipped with appropriate initial and boundary conditions. The dimensionless parameters characterizing the problem are the Reynolds number Re, the Froude number Fr and the Peclet number Pe. We set $Re = 10$, $Fr = 1/150$, and $Pe = 20/3$. The vector $\hat{g}$ represents the normalized gravitational acceleration. We have $\hat{g} = (0, -1)^T$ for our benchmark problem.

The fluid of the laminar flow is suddenly heated from below with constant temperature $T_b = 1.0$ at the bottom wall, whereas the top wall is maintained at temperature $T_t = 0$. For $x_1 = 0$, we impose a linear distribution of the temperature, i.e., $T(t, 0, x_2) = 1 - x_2$, which is the same linear function as for the initial condition. For the velocity, we prescribe a parabolic inflow profile at the inlet given by

$$u_1(t, 0, x_2) = 6x_2(1 - x_2)\,, \qquad u_2(t, 0, x_2) = 0\,,$$

and no-slip boundary conditions at the top and bottom wall. The initial condition is equivalent to the parabolic inflow profile. At the right outflow boundary non-flux conditions are imposed for velocity and temperature.

The performance of the different solvers for the benchmark problem is measured by means of the time- and space-averaged Nusselt numbers at the top and bottom boundary. We define the Nusselt numbers by [4]

$$Nu_b = \frac{1}{L(t_2 - t_1)} \int_{t_1}^{t_2} \int_0^{10} -\frac{\partial T}{\partial x_2}(t, x_1, 0)\, dx_1\, dt\,,$$

and

$$Nu_t = \frac{1}{L(t_2 - t_1)} \int_{t_1}^{t_2} \int_0^{10} -\frac{\partial T}{\partial x_2}(t, x_1, 1)\, dx_1\, dt\,,$$

for the time interval $[t_1, t_2] = [3, 15]$. L is defined by the ratio of length and height of the domain Ω, i.e., $L = 10$.

3 TIME AND SPACE DISCRETIZATION

We first discretize (2.1) in time with an s-stage linearly implicit two-step peer method [5]. Afterwards, stabilized linear finite elements [8] are used for the space discretization.

Let $\tau_m > 0$ be a variable time step. Then, an approximation $V_{mi} = (P_{mi}, U_{mi}, T_{mi})^T$ to the exact solution at time $t_{mi} := t_m + c_i\tau_m$ with $t_m = t_{m-1,s}$ for $m \geq 1$ and $c_i \in [-1,1]$, $c_s = 1$, can be computed from the recursive form

$$\begin{aligned}
\nabla(P_{mi} - P^0_{mi}) + \left(\frac{I}{\tau_m\gamma} - \frac{1}{Re}\Delta + U_{m-1,s}\cdot\nabla\right)(U_{mi} - U^0_{mi}) & \\
+ ((U_{mi} - U^0_{mi})\cdot\nabla)U_{m-1,s} + \frac{1}{Fr}(T_{mi} - T^0_{mi})\hat{g} & \\
= -\nabla P^0_{mi} - \left(U^0_{mi}\cdot\nabla - \frac{1}{Re}\Delta\right)U^0_{mi} - \frac{1}{Fr}T^0_{mi}\hat{g} & \\
+ \frac{1}{\tau_m\gamma}(w_{U,i} - U^0_{mi})\,, & \qquad (3.2a)\\
\nabla\cdot(U_{mi} - U^0_{mi}) = -\nabla\cdot U^0_{mi}\,, & \qquad (3.2b)\\
((U_{mi} - U^0_{mi})\cdot\nabla)T_{m-1,s} + \left(\frac{I}{\tau_m\gamma} - \frac{1}{Pe}\Delta + U_{m-1,s}\cdot\nabla\right)(T_{mi} - T^0_{mi}) & \\
= -(U^0_{mi}\cdot\nabla)T^0_{mi} + \frac{1}{Pe}\Delta T^0_{mi} + \frac{1}{\tau_m\gamma}(w_{T,i} - T^0_{mi}) & \qquad (3.2c)
\end{aligned}$$

for $i = 1,\ldots,s$, with the corresponding boundary conditions taken at t_{mi}. The internal values $w_i = (w_{P,i}, w_{U,i}, w_{T,i})^T$ are defined by

$$w_i = \sum_{j=1}^{i-1}\frac{1}{\gamma}a_{ij}(V_{mj} - w_j) + \sum_{j=1}^{s}u_{ij}(\sigma_m)V_{m-1,j}$$

and the predictors by

$$V^0_{mi} = \sum_{j=1}^{i-1}\frac{1}{\gamma}a^0_{ij}(V_{mj} - w_j) + \sum_{j=1}^{s}u^0_{ij}(\sigma_m)V_{m-1,j}\,.$$

The above system is first solved for the differences $\hat{P}_{mi} = P_{mi} - P^0_{mi}$, $\hat{U}_{mi} = U_{mi} - U^0_{mi}$, $\hat{T}_{mi} = T_{mi} - T^0_{mi}$, and these values are than updated by using the predictors. The numerical solution at time t_{m+1} is given by the last stage values P_{ms}, U_{ms}, and T_{ms}.

We choose stretched Chebychev nodes

$$c_i := -\frac{\cos\left(\left(i - \frac{1}{2}\right)\frac{\pi}{s}\right)}{\cos\left(\frac{\pi}{2s}\right)}\,, \quad i = 1,\ldots,s$$

for the abscissa $c \in \mathbb{R}^s$. The coefficients a_{ij} can be combined in a lower triangular matrix $A \in \mathbb{R}^{s\times s}$ with positive diagonal elements $a_{ii} = \gamma$, the coefficients u_{ij} build a possibly full matrix $U \in \mathbb{R}^{s\times s}$. The matrix U depends on the step size ratio $\sigma_m = \tau_m/\tau_{m-1}$ because of the order conditions of the method for variable step sizes. For the real coefficients of the predictor, similar properties are valid:

$$A^0 = (a^0_{ij}) \quad \text{with} \quad a^0_{ij} = 0 \quad \text{for} \quad i \leq j \quad \text{and} \quad U^0 = (u^0_{ij}(\sigma_m))\,.$$

Using an appropriate set of coefficients, we get order $s-1$ for variable time steps and order s for constant time steps [5].

A variable step size approach based on an embedding strategy is used to increase the efficiency of the methods. A linear combination of the V_{mi}, $i = 1,\ldots,s-1$, yields a second solution $\tilde{V}_{ms}$ of inferior order $\tilde{p} = s-2$, which serves for an approximation of the local error

$$ERR_t := \left(\frac{1}{n}\sum_{i=1}^{n}\frac{\|V_{ms} - \tilde{V}_{ms}\|^2_{L^2}}{\left(ScalR_i\|e_i^T V_{ms}\|_{L^2} + ScalA_i\sqrt{|\Omega|}\right)^2}\right)^{\frac{1}{2}}\,.$$

$ScalR_i$ and $ScalA_i$ are parameters for the relative and absolute scaling factors, respectively. Let TOL_t denote the desired time tolerance. The new time step size is then given by

$$\tau_{\text{new}} = \min\{\tau_{\max}, \min\{2, \max\{0.2, (TOL_t/ERR_t)^{1/(\tilde{p}+1)}\}\} \times 0.9\tau_m\} .$$

A description in more detail can be found in Gerisch et al. [5].

We solve the time-independent spatial problems (3.2) by a linear finite element method [8] on a triangular mesh $\mathcal{T}^h$ with characteristic length size h. Let S_h^1 denote the space of piecewise linear continuous functions over $\mathcal{T}^h$. For the differences $\hat{P}_{mi}$, $\hat{U}_{mi}$ and $\hat{T}_{mi}$, the standard Galerkin finite element solutions $\hat{P}_{mi}^h \in S_h^1$, $\hat{U}_{mi}^h \in S_h^1 \times S_h^1$ and $\hat{T}_{mi}^h \in S_h^1$ are given by the equations

$$\begin{aligned}
-\left(\hat{P}_{mi}^h, \nabla\cdot\varphi_u\right) + \frac{1}{\tau_m\gamma}\left(\hat{U}_{mi}^h, \varphi_u\right) + \frac{1}{Re}\left(\nabla\hat{U}_{mi}^h, \nabla\varphi_u\right) + \left((U_{m-1,s}^h\cdot\nabla)\hat{U}_{mi}^h, \varphi_u\right) \\
+ \left((\hat{U}_{mi}^h\cdot\nabla)U_{m-1,s}^h, \varphi_u\right) + \frac{1}{Fr}\left(\hat{T}_{mi}^h\,\hat{g}, \varphi_u\right) \\
= \left(P_{mi}^{0,h}, \nabla\cdot\varphi_u\right) - \left((U_{mi}^{0,h}\cdot\nabla)U_{mi}^{0,h}, \varphi_u\right) - \frac{1}{Re}\left(\nabla U_{mi}^{0,h}, \nabla\varphi_u\right) \\
- \frac{1}{Fr}\left(T_{mi}^0\,\hat{g}, \varphi_u\right) + \frac{1}{\tau_m\gamma}\left(w_{U,i}^h, \varphi_u\right) - \frac{1}{\tau_m\gamma}\left(U_{mi}^{0,h}, \varphi_u\right) , \qquad (3.3a)
\end{aligned}$$

$$\left(\nabla\cdot\hat{U}_{mi}^h, \varphi_p\right) = -\left(\nabla\cdot U_{mi}^{0,h}, \varphi_p\right) , \qquad (3.3b)$$

$$\begin{aligned}
\left((\hat{U}_{mi}^h\cdot\nabla)T_{m-1,s}^h, \varphi_T\right) + \frac{1}{\tau_m\gamma}\left(\hat{T}_{mi}^h, \varphi_T\right) + \frac{1}{Pe}\left(\nabla\hat{T}_{mi}^h, \nabla\varphi_T\right) + \left((U_{m-1,s}^h\cdot\nabla)\hat{T}_{mi}^h, \varphi_T\right) \\
= -\left((U_{mi}^{0,h}\cdot\nabla)T_{mi}^{0,h}, \varphi_T\right) - \frac{1}{Pe}\left(\nabla T_{mi}^{0,h}, \nabla\varphi_T\right) + \frac{1}{\tau_m\gamma}\left(w_{T,i}^h, \varphi_T\right) \\
- \frac{1}{\tau_m\gamma}\left(T_{mi}^{0,h}, \varphi_T\right) \qquad (3.3c)
\end{aligned}$$

for all $\varphi_u \in S_h^1 \times S_h^1$, $\varphi_p \in S_h^1$, and $\varphi_T \in S_h^1$. Here, $(\cdot,\cdot)$ is the usual inner product in $L^2(\Omega)$.

Since we use the same finite element functions for pressure and velocity, a relaxation of the incompressibility condition

$$\nabla\cdot u = \delta_T \nabla\cdot\left(\partial_t u + (u\cdot\nabla)u - \frac{1}{Re}\Delta u + \nabla p + \frac{1}{Fr}T\,\hat{g}\right) \qquad (3.4)$$

is necessary to avoid spurious pressure modes of the numerical solution. Note that the term on the right hand side is identically zero. The parameter δ_T is locally defined on each triangle $T \in \mathcal{T}^h$ through [8]

$$\delta_T = c\frac{h_b}{2u_{\text{ref}}}\frac{\hat{Re}}{\sqrt{1+\hat{Re}^2}} , \qquad \hat{Re} = h_b u_{\text{ref}} Re , \qquad c = 0.4$$

for a global reference velocity u_{ref} and the diameter h_b of the two-dimensional ball which is area-equivalent to the element T. For our benchmark problem, we use $u_{\text{ref}} = 1$. Consequently, we have

to replace (3.3b) by a discrete version of (3.4). Using partial integration for the divergence term on the right hand side it reads

$$\begin{aligned}
\left(\nabla\cdot\hat{U}^h_{mi},\varphi_p\right) + \sum_{T\in\mathscr{T}^h}\delta_T\Big\{&\left(\nabla\hat{P}^h_{mi},\nabla\varphi_p\right)_T + \frac{1}{\tau_m\gamma}\left(\hat{U}^h_{mi},\nabla\varphi_p\right)_T \\
&-\frac{1}{Re}\left(\Delta\hat{U}^h_{mi},\nabla\varphi_p\right)_T + \left((U^h_{m-1,s}\cdot\nabla)\hat{U}^h_{mi},\nabla\varphi_p\right)_T \\
&+\left((\hat{U}^h_{mi}\cdot\nabla)U^h_{m-1,s},\nabla\varphi_p\right)_T + \frac{1}{Fr}\left(\hat{T}^h_{mi}\,\hat{g},\nabla\varphi_p\right)_T\Big\} \\
= -\left(\nabla\cdot U^{0,h}_{mi},\varphi_p\right) + \sum_{T\in\mathscr{T}^h}\delta_T\Big\{&-\left(\nabla P^{0,h}_{mi},\nabla\varphi_p\right)_T \\
&-\left((U^{0,h}_{mi}\cdot\nabla)U^{0,h}_{mi},\nabla\varphi_p\right)_T + \frac{1}{Re}\left(\Delta U^{0,h}_{mi},\nabla\varphi_p\right)_T \\
&-\frac{1}{Fr}\left(T^0_{mi}\,\hat{g},\nabla\varphi_p\right)_T + \frac{1}{\tau_m\gamma}\left(w^h_{U,i},\nabla\varphi_p\right)_T - \frac{1}{\tau_m\gamma}\left(U^{0,h}_{mi},\nabla\varphi_p\right)_T\Big\}
\end{aligned} \tag{3.5}$$

for all $\varphi_p \in S^1_h$. We note that in our setting, the second order terms $\Delta\hat{U}^h_{mi}$ and $\Delta\hat{U}^{0,h}_{mi}$ vanish since linear elements are used.

4 NUMERICAL RESULTS

We apply the two-step peer methods PEER4 and PEER5 [5], which have order three and four for variable step sizes, to solve the benchmark problem (2.1) and study the accuracy and efficiency of these methods compared to the linearly implicit one-step Rosenbrock methods ROS3P [10] and ROS3PL [9] of classical order three. The second-order method ROS2 [2] is also included in the simulations to obtain a comparison to the widely-used Crank-Nicolson method, which is quite similar to ROS2. For the spatial discretization, an unstructured mesh consisting of 76,087 triangles is used. We have used the facilities of the fully space-time adaptive solver KARDOS to a priori design a spatial discretization that guarantees a relative spatial accuracy of nearly 10^{-4} over the whole time interval.

For small values of the Rayleigh number, $Ra = RePe/Fr = 10,000$ in our case, the Poiseuille flow results in a thermo-convective instability, where travelling transverse waves occur with axes perpendicular to the main flow direction [1], see Fig. 1. The irregular behaviour of the fluid at the right boundary can also

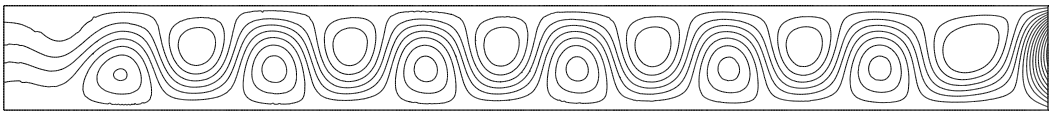

(a) Streamlines

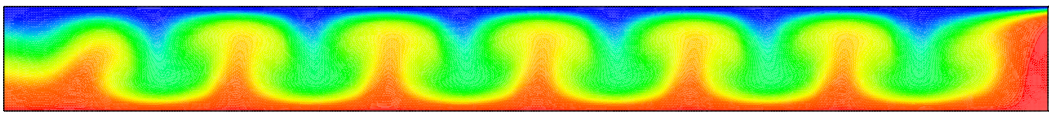

(b) Temperature contours

Figure 1: Streamlines and temperature contours at time $t = 8.90$.

be observed in this figure, which raises the question if the boundary condition at the outlet represents the infinitely long channel correctly. The appropriate setting of boundary conditions for the numerical simulation of flows in infinite domains is still a great challenge. However, the artificial boundary conditions do not have an impact on the numerical solution for $2 \le x_1 \le 8$, which was observed by Evans and Paolucci [4].

We computed the following reference values for the Nusselt number at the bottom and top boundary

$$Nu_b = 2.400353\,, \qquad Nu_t = 2.575916\,,$$

which result from simulations with decreasing constant step sizes for all methods. The reference values are converged up to the sixth decimal and equal for all methods considered. The reference value Nu_t at the top boundary is comparable to the value obtained by Evans and Paolucci [4]. There Nu_b was not considered.

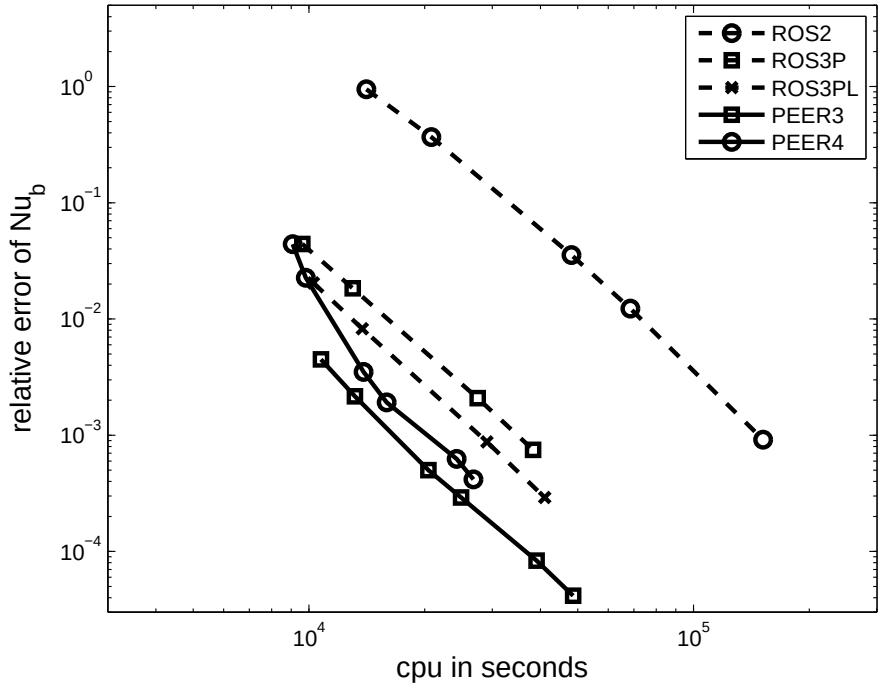

Figure 2: **Nusselt number at bottom boundary.** The relative error of the Nusselt number at the bottom boundary of the plane Poiseuille flow is presented for peer and Rosenbrock solvers. The requested time tolerances are $10^{-2}, 5\times10^{-3}, \ldots, 5\times10^{-5}$.

Time-adaptive simulations are performed for the comparison of the one- and two-step solvers considered, where tolerances of $10^{-2}, 5\times10^{-3}, \ldots, 5\times10^{-5}$ for the peer methods and Rosenbrock methods are required. Fig. 2 and Fig. 3 relate the relative error of the computed Nusselt numbers at the bottom and top boundary to the CPU time in seconds. The higher accuracy and better efficiency of PEER4 and PEER5 compared to the Rosenbrock methods are obvious. PEER4 delivers the best results. The relatively poor performance of ROS2, which is clearly outperformed by the peer methods and also by the other third-order methods, shows the usefulness of higher order approximations for the thermo-convective benchmark problem.

5 CONCLUSIONS

A numerical solution of thermally coupled benchmark flow is provided by two linearly implicit two-step peer methods and three one-step Rosenbrock methods combined with finite element methods to discretize in space. We could observe that the peer method PEER4, which has order three for variable time steps and order four for constant time steps, performs very well compared to the other Rosenbrock solvers tested. It clearly outperforms the second order method ROS2, which is similar to the well-known Crank-Nicolson method, by several orders of magnitude. The second two-step peer method, PEER5,

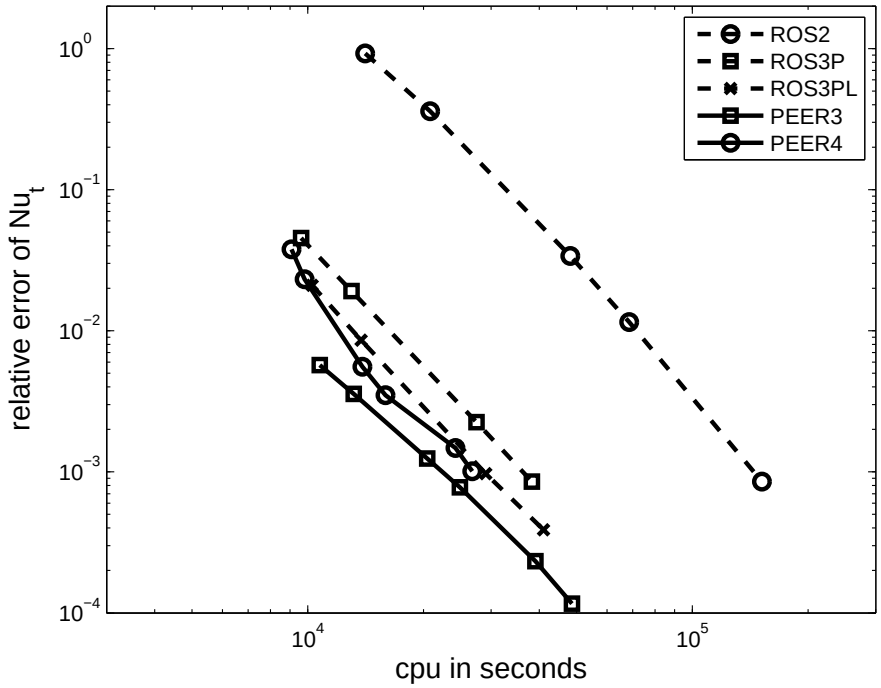

Figure 3: **Nusselt number at top boundary.** The relative error of the Nusselt number at the top boundary of the plane Poiseuille flow is presented for peer and Rosenbrock solvers. The requested time tolerances are $10^{-2}, 5 \times 10^{-3}, \ldots, 5 \times 10^{-5}$.

still performs well but less efficient than PEER4. We conclude that two-step peer methods recommend themselves as good candidates for CFD computations that demand for high resolution.

6 ACKNOWLEDGEMENT

This work is supported by the Deutsche Forschungsgemeinschaft within the Graduate College "Instationary system modelling of aircraft turbines".

Bibliography

[1] R. Codina and J. Principe, Dynamic subscales in the finite element approximation of thermally coupled incompressible flows. *Int. J. Numer. Meth. Fluids*, **54**, 707–730 (2007).

[2] K. Dekker and J.G. Verwer, Stability of Runge-Kutta methos for stiff nonlinear differential equations, North-Holland Elsevier Science Publishers, 1984.

[3] B. Erdmann, J. Lang and R. Roitzsch, KARDOS user's guide. Tech. Rep. ZR 02–42, Konrad-Zuse-Zentrum Berlin, 2002.

[4] G. Evans and S. Paolucci, The thermoconvective instability of plane Poiseuille flow heated from below: a proposed benchmark solution for open boundary flows. *Int. J. Numer. Meth. Fluids*, **11**, 1001–1013 (1990).

[5] A. Gerisch, J. Lang, H. Podhaisky and R. Weiner, High-order linearly implicit two-step peer — finite element methods for time-dependent PDEs. *Appl. Numer. Math.*, **59**, 624–638 (2009).

[6] B. Gottermeier, J. Lang, Adaptive two-step peer methods for incompressible Navier-Stokes equations. Tech. Rep. 2592, Technische Universität Darmstadt, 2009. — to appear in Proceedings of ENUMATH 2009, Springer-Verlag.

[7] V. John, J. Rang, Adaptive time step control for the incompressible Navier-Stokes equations. *Comput. Meth. Appl. Mech. Engrg.*, **199**, 514–524 (2010).

[8] J. Lang, Adaptive incompressible flow computations with linearly implicit time discretization and stabilized finite elements. In: K. D. Papailiou, D. Tsahalis, J. Periaux, C. Hirsch and M. Pandolfi (eds.) *Computational Fluid Dynamics*, pp. 200–204, John Wiley & Sons, New York (1998).

[9] J. Lang, D. Teleaga, Towards a fully space-time adaptive FEM for magnetoquasistatics. *IEEE Trans. Magn.*, **44**, 1238–1241 (2008).

[10] J. Lang, J. Verwer, ROS3P — an accurate third-order Rosenbrock solver designed for parabolic problems. *BIT*, **41**, 731–738 (2001).